
RCDN: Towards Robust Camera-Insensitivity Collaborative Perception via Dynamic Feature-based 3D Neural Modeling

Tianhang Wang
Tongji University
tianya_wang@tongji.edu.cn

Fan Lu
Tongji University
lufan@tongji.edu.cn

Zehan Zheng
Tongji University
zhengzehan@tongji.edu.cn

Guang Chen*
Tongji University
guangchen@tongji.edu.cn

Changjun Jiang
Tongji University
cjjiang@tongji.edu.cn

Abstract

Collaborative perception is dedicated to tackling the constraints of single-agent perception, such as occlusions, based on the multiple agents' multi-view sensor inputs. However, most existing works assume an ideal condition that all agents' multi-view cameras are continuously available. In reality, cameras may be highly noisy, obscured or even failed during the collaboration. In this work, we introduce a new robust camera-insensitivity problem: *how to overcome the issues caused by the failed camera perspectives, while stabilizing high collaborative performance with low calibration cost?* To address above problems, we propose **RCDN**, a **R**obust **C**amera-insensitivity collaborative perception with a novel **D**ynamic feature-based **3D** **N**eural modeling mechanism. The key intuition of RCDN is to construct collaborative neural rendering field representations to recover failed perceptual messages sent by multiple agents. To better model collaborative neural rendering field, RCDN first establishes a geometry BEV feature based time-invariant static field with other agents via fast hash grid modeling. Based on the static background field, the proposed time-varying dynamic field can model corresponding motion vectors for foregrounds with appropriate positions. To validate RCDN, we create OPV2V-N, a new large-scale dataset with manual labelling under different camera failed scenarios. Extensive experiments conducted on OPV2V-N show that RCDN can be ported to other baselines and improve their robustness in extreme camera-insensitivity settings. Our code and datasets will be available soon.

1 Introduction

Multi-agent collaborative perception[1–5] obtains better and more holistic perception by allowing multiple agents to exchange complementary perceptual information. This field has the potential to effectively address various persistent challenges in single-perception, such as occlusion[6, 7]. The associated techniques and systems also process significant promise in various domains, such as the utilization of multiple unmanned aerial aircraft for search and rescue operations[8–10], the automation and mapping of multiple robots[11–13]. As an emerging field, the research of collaborative perception faces several issues that need to be addressed. These challenges include the need for high-quality datasets[14–17], the formulation of models that are agnostic to specific tasks and models[18, 19], and the ability to handle pose error and adversarial attacks[20, 21].

*Corresponding Author

However, a vast majority of existing works do not seriously account for the harsh realities[22, 23] of real-world sensors in the collaboration, such as blurred, high noise, interruption and even failure. These factors directly undermine the basic collaboration premise[24, 25] of reconstructing the holistic view based on the multi-view sensors that severely impact the reliability and quality of collaborative perception process. This raises a critical inquiry: *how to overcome the issues caused by the failed cameras’ perspectives while stabilizing high collaborative performance with low calibration cost?* The designation *camera insensitivity* overcomes the unpredictable essence of the specific failure camera numbers and time; see Figure 1 for an illustration. To address this issue, one viable solution is adversarial defense[26]. By robust defense strategy, adversarial defense bypasses camera insensitivity among blurred and noise. However, its performance is suboptimal[27] and has been shown to be particularly vulnerable to noise ratios[20] and failed camera numbers.

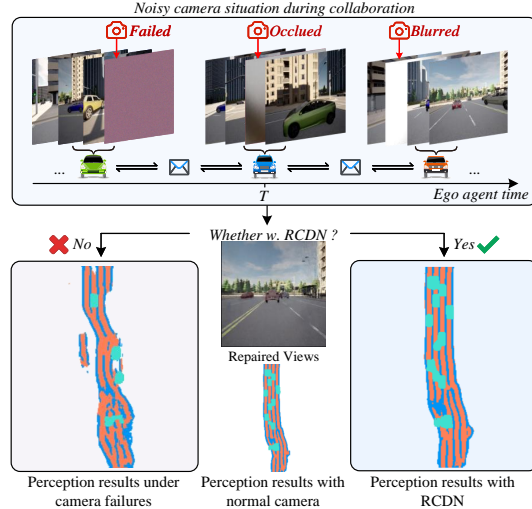


Figure 1: Illustration of noisy camera situations (blurred, occluded and even failed) during collaboration and the perception result *w.o./w.* RCDN. orange for drivable areas segmentation, blue for lanes and teal for dynamic vehicles.

To address this robust camera insensitivity collaborative perception problem, we propose **RCDN**, a **R**obust **C**amera-insensitivity collaborative perception with a **D**ynamic feature-based 3D **N**eural modeling mechanism. The core idea is to recover noisy camera perceptual information from other agents’ views by modeling the collaborative neural rendering field representations. Specifically, RCDN has two collaborative field phases: a time-invariant static background field and time-varying dynamic foreground field. In the static phases, RCDN sets other baselines’ backbone as the collaboration base and undertakes end-to-end training to create a robust unified geometry BEV feature space for all agents. Then, the geometry BEV feature combines the hash grid modeling, an explicit and multi-resolution network, to generate static background views through α -composed accumulation of RGB values along a ray at a fast speed. In the dynamic phase, RCDN utilizes 4D spatiotemporal position features to model the dynamic motion of 3D points, which learns an accurate motion field under optical priors and spatiotemporal regularization. The proposed RCDN has two major advantages: i) RCDN can handle camera insensitivity collaboration under unknown noisy timestamps and numbers; ii) RCDN does not put any extra communication burden into inference stage and costs little computation burden.

In our efforts to validate the effectiveness of RCDN, we identified a gap: the lack of a comprehensive collaborative perception dataset that accounts for different camera noise scenarios. To address this, we create the OPV2V-N, an expansive new dataset derived from OPV2V, featuring meticulously labeled timestamps and camera IDs. This advancement aims to support and enhance research in camera-insensitive collaborative perception. Extensive experiments on OPV2V-N show RCDN’s remarkable performance when other baselines equipped with RCDN under extreme camera-insensitivity setting, improving *w.o.* RCDN baseline methods by about 157.91%.

2 Related Works

Robust Single Perception. Single-agent perceptions[28, 29, 27, 30–32] have tackled the robust camera setting with other sensor modals. [27] reveals that camera-based methods [32] can be easily effected by camera working conditions. Some works[30, 29] introduce LiDAR into perception system and design a soft-association mechanism between the LiDAR and the inferior camera-side, to relieve the negative impacts caused by cameras. MVX-Net[31] improves the combination pipeline of LiDAR and cameras by leveraging the VoxelNet[33] architecture. CRN[28] introduces the low-cost Radar to replace the LiDAR, which can provide precise long-range measurement and operates reliably in all environments. However, as for the camera-only situation, few work seeks to solve this because recovering just from the single-view is highly ill-posed (with infinitely many solutions that match the

input image). With the recent rapid development of V2X[34], we now can introduce the multi-agent and multi-view based collaborative perception setting to explore this extreme situation.

Collaborative Perception. Perception tasks for single agents can be adversely affected by factors such as limited sensor fields of view and physical ambient occlusions. To address the aforementioned challenges, collaborative perception[35–37] can attain more comprehensive perceptual output by exchanging perception data. Early techniques involved the transmission of either unprocessed sensory input (referred to as early fusion) or the results of perception (referred to as late fusion). Nevertheless, recent research has been examining the transfer of intermediate features to achieve a balance between performance and bandwidth. Some works[38–41] devote selecting the most informative messages to communicate. DiscoNet[42] utilizes knowledge distillation to achieve a better trade-off between performance and bandwidth. V2X-ViT[43] presents a unified V2X framework based on Transformer that takes into account the heterogeneity of V2X system. Meanwhile, some learnable or mathematical based methods[44–47] have also been proposed to correct the pose errors and latency. Moreover, some works[48, 49] reveal that the holistic character of collaborative perception can improve the effect of driving planning and control tasks. However, most existing papers do not take the harsh realities of real-world sensors into account, such as blurred, high noise, occlusion and even failure, which directly undermine the basic collaboration premise of multi-view based modeling, negatively impacting performance. This work formulates camera-insensitivity collaborative perception, which considers real-world camera sensor conditions.

Neural Rendering. Neural radiance fields[50] aim to utilize implicit neural representations to encode densities and colors of the scene. This approach takes advantage of volumetric rendering to synthesize views, and it can be effectively optimized from 2D multi-view images. Hence, numerous works have enhanced NeRF in terms of rendering quality[51–53], efficiency[54–57], *etc.* For example, Mip-NeRF[58] utilizes cone tracing instead of ray tracing in standard NeRF volume rendering by introducing integrated positional encoding, which greatly improves the render quality. To improve the efficiency of training and inference processes, Instant-NGP[59] proposes a learned parametric multi-resolution hash for efficient encoding, which also leads to high compactness. Some works have also extended NeRF to large-scale urban autonomous scenes[60–62]. In this work, we first introduce neural rendering to collaborative perception. The proposed collaborative neural rendering field representations will address the problem of recovering highly noisy perceptual messages.

3 Problem Formulation

Consider N agents in a scene, where each agent can send and receive collaboration messages from other agents. For the n -th agent, let $\mathcal{X}_n^{t_i} = \{\mathcal{I}_c^{t_i}\}_{c=1}^{c_n}$ and $\mathcal{Y}_n^{t_i}$ be the raw observation and the perception ground-truth at time current t_i , respectively, where $\mathcal{I}_c^{t_i}$ is the c -th camera images recorded at i -th timestamp, and $\mathcal{P}_{m \rightarrow n}^{t_i}$ is the collaboration message sent from the agent m at time t_i . The key of the camera insensitivity is that the specific noisy camera number and corresponding timestamp are unpredictable. Therefore, each agent has to encounter invalid view information, which contains both local observation and collaboration messages sent from other agents. Then, the task of camera insensitivity collaborative perception is formulated as:

$$\begin{aligned} \max_{\theta_1, \theta_2, \mathcal{P}} \quad & \sum_{n=1}^N g(\hat{\mathbf{Y}}_n^{t_i}, \mathbf{Y}_n^{t_i}) \\ \text{subject to} \quad & \hat{\mathbf{Y}}_n^{t_i} = \mathbf{c}_{\theta_2}(\boldsymbol{\pi}_{\theta_1}(\psi(\mathcal{X}_n^{t_i}, \{\mathcal{P}_{m \rightarrow n}^{t_i}\}_{m=1}^{N-1}))), \end{aligned} \quad (1)$$

where $g(\cdot, \cdot)$ is the perception evaluation metrics, $\hat{\mathbf{Y}}_n^{t_i}$ is the perception result of the n -th agent at time t_i , $\psi(\cdot, \cdot)$ is the camera noise function to simulate the harsh realities of the real-world situation, $\boldsymbol{\pi}_{\theta_1}(\cdot)$ is the proposed collaborative neural rendering field network RCDN with trainable parameters θ_1 , and \mathbf{c}_{θ_2} is the existing collaborative perception network with trainable parameters θ_2 . Note that the proposed RCDN is to recover the noisy camera views caused by the ψ function, making collaborative perception system more robust to the unpredictable situation of noisy camera data.

Given such high noisy camera view, the performances of collaborative perception system would be significantly degraded since the mainstream collaborative perception utilizes the multi-view camera-based BEV features for communication and downstream tasks, and using such damaged features

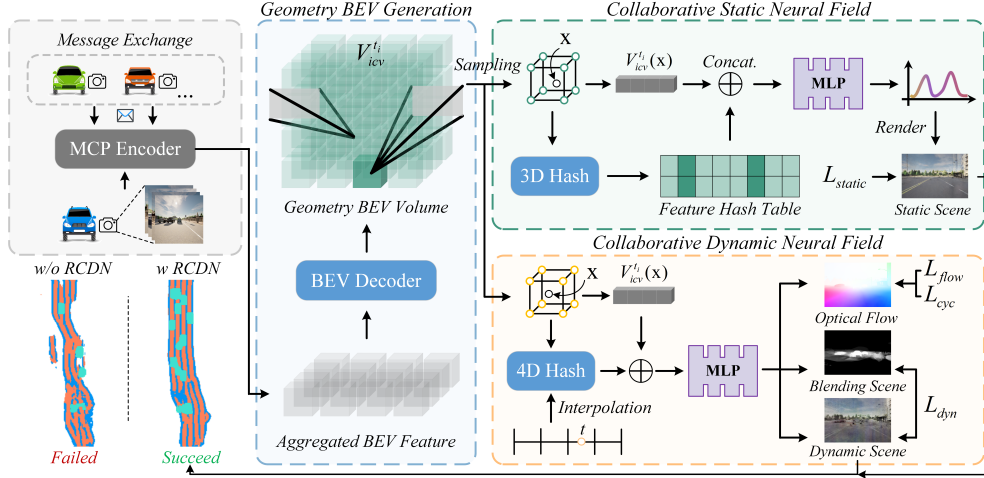


Figure 2: System overview. The geometry BEV generation module provides feature sampling for later processes. The collaborative static and dynamic fields are performed in parallel to model the background and foreground, respectively. Note that MCP is short for the multi-agents collaborative perception process.

would contain erroneous information during the perception process. In the next section, we will introduce RCDN to address this issue.

4 RCDN

This section proposes a robust camera-insensitivity collaborative perception system, RCDN. Figure 2 overviews the framework of the RCDN module in Sec.4.1. The details of three key modules of RCDN can be found in Sec.4.2-4.4.

4.1 Overall Architecture

The problem of noisy camera view results in the sub-optimization of the holistic multi-view based BEV features generation in the collaboration messages. That is, the collaboration messages from both self and other agents would be noisy or damaged for the fusion process. The proposed RCDN addresses this issue with two key notions: i) we construct novel collaborative neural rendering field representations, enabling collaborative perception to recover from the noisy camera view; and ii) we establish time-invariant and time-varying fields for background and foreground, respectively, making the collaborative neural rendering field more accurate.

Mathematically, let the n -th agent be the ego agent and $\mathcal{X}_n^{t_i}$ be its raw observation at the t_i timestamp of agent n . The proposed camera-insensitivity collaborative perception system RCDN is formulated as follows:

$$\mathbf{F}_n^{t_i} = f_{\text{enc}}(\psi(\mathcal{X}_n^{t_i}, \{\mathcal{X}_j^{t_i}\}_{j=1}^{N-1})), \quad (2a)$$

$$\mathbf{V}_{icv}^{t_i} = f_{\text{geo_bev}}(\mathbf{F}_n^{t_i}), \quad (2b)$$

$$(\sigma^s, \mathbf{c}^s) = f_{\text{static}}(\mathbf{r}(u_k), \mathbf{V}_{icv}^{t_i}(\mathbf{r}(u_k))), \quad (2c)$$

$$(\mathbf{s}_{fw}, \mathbf{s}_{bw}, \sigma_{t_i}^d, \mathbf{c}_{t_i}^d, \mathbf{b}) = f_{\text{dynamic}}(\mathbf{r}(u_k), \mathbf{V}_{icv}^{t_i}(\mathbf{r}(u_k)), t_i), \quad (2d)$$

$$\tilde{\mathcal{X}}_n^{t_i}, \{\tilde{\mathcal{X}}_j^{t_i}\}_{j=1}^{N-1} = f_{\text{render}}(\sigma^s, \mathbf{c}^s, \sigma_{t_i}^d, \mathbf{c}_{t_i}^d, \mathbf{b}), \quad (2e)$$

$$\hat{\mathbf{Y}}_n^{t_i} = f_{\text{mcp}}(\tilde{\mathcal{X}}_n^{t_i}, \{\tilde{\mathcal{X}}_j^{t_i}\}_{j=1}^{N-1}), \quad (2f)$$

where $\mathbf{F}_n^{t_i} \in \mathbb{R}^{C \times H \times W}$ is the BEV feature maps of the n -th agent at timestamp t_i with H, W the size of BEV map and C the number of channels; $\mathbf{V}_{icv}^{t_i} \in \mathbb{R}^{C \times Z \times H \times W}$ is the implicit collaborative geometry volume feature of the scenarios; which is lifted from BEV plane with the Z height; $\mathbf{r}(u(k))$ is the ray from the failed camera center $\mathbf{o} \in \mathbb{R}^2$ through a given pixel on the image plane as $\mathbf{r}(u(k)) = \mathbf{o} + u(k)\mathbf{d}$, where $\mathbf{d} \in \mathbb{R}^3$ is the normalized viewing direction; f_{static} is a explicit hash grid based representation to model the collaborative static scenarios volume density $\sigma^s \in \mathbb{R}^1$ and corresponding color $\mathbf{c}^s \in \mathbb{R}^3$; f_{dynamic} is the dynamic collaborative neural network

takes the interpolated 4D-tuple $(\mathbf{r}(u(k)), t_i)$ and sampled $\mathbf{V}_{icv}^{t_i}$ feature as input and predict 3D collaborative scene flow vectors $\mathbf{s}_{fw}, \mathbf{s}_{bw} \in \mathbb{R}^3$, dynamic volume density $\sigma_{t_i}^d$, color $\mathbf{c}_{t_i}^d$ and blending weight $\mathbf{b} \in \mathbb{R}^2$; and $\{\tilde{\mathcal{X}}_n^{t_i}, \{\tilde{\mathcal{X}}_j^{t_i}\}_{j=1}^{N-1}\}$ is the recovered noisy camera images at timestamp t_i after collaborative rendering; and $\tilde{\mathbf{Y}}_n^{t_i}$ is the final output of the system. In summary, Step 2a extracts BEV perceptual features from observation data. Step 2b generates the collaborative geometry BEV volume feature map for each timestamp, enabling feature sampling in Step 2c and 2d. Step 2d models the static background field of collaboration scenarios. Step 2d models the dynamic foreground field of collaboration objects. Step 2e gets the global volume density and color information by combining both static and dynamic field models to recover the failed camera perspective images. Finally, Step 2f outputs the final perceptual results with repaired images.

Note that i) Step 2a is done locally, Step 2b-2f are performed after receiving the messages from others. The proposed RCDN does not require any extra transmission during the inference process, which is bandwidth friendly; and ii) Step 2c and 2d are performed in parallel to save inference time; and iii) Same as [42, 47], RCDN adopts the feature representations in bird’s eye view (BEV), where the feature maps of all agents are projected to the same global coordinate system. We now elaborate on the details of Steps 2b-2e in the following subsections.

4.2 Collaborative Geometry BEV Volume Feature

Given the BEV feature map of each agent, Step 2b aims to construct a unified collaborative geometry BEV volume feature for each timestamp of the scenario. The intuition is that [63] points out that combing with generic feature representations can avoid the per-scene "network memorization" phenomenon[50], which will improve the efficiency of the optimization process. Therefore, using the geometry BEV feature can enable the subsequent Step 2c, 2d to learn more generic networks for both static and dynamic collaborative neural fields, respectively.

To implement, we use a geometry-aware decoder D_{geo} to transform the BEV feature $\mathbf{F}_n^{t_i}$ into the intermediate feature $\mathbf{F}_n^{t_i} \in \mathbb{R}^{C \times 1 \times X \times Y}$ and $\mathbf{F}_{height,n}^{t_i} \in \mathbb{R}^{1 \times Z \times X \times Y}$, and this feature is lifted from BEV plane to an implicit collaborative volume feature $\mathbf{V}_{icv}^{t_i} \in \mathbb{R}^{C \times Z \times X \times Y}$:

$$\mathbf{V}_{icv}^{t_i} = \text{sigmoid}(\mathbf{F}_{height,n}^{t_i}) \cdot \mathbf{F}_n^{t_i}, \quad (3)$$

where \cdot represents dot production along the channel. Eq. 3 lifts the items on the BEV plane into 3D collaborative volume with the estimated height position $\text{sigmoid}(\mathbf{F}_{height,n}^{t_i})$. $\text{sigmoid}(\mathbf{F}_{height,n}^{t_i})$ represents whether there is an item at the corresponding height. Ideally, the collaborative volume feature $\mathbf{V}_{icv}^{t_i}$ contains all the scene items information in the corresponding position.

4.3 Static Collaborative Neural Field

After getting the collaborative volume feature $\mathbf{V}_{icv}^{t_i}$, Step 2c aims to construct the background of camera views with the static collaborative neural field. Given an arbitrary 3D scenario position $\mathbf{x} \in \mathbb{R}^3$ and a 2D viewing direction $\mathbf{d} \in \mathbb{R}^2$, we aims to estimate static scenarios volume density σ^s and emitted RGB color \mathbf{c}^s using the fast hash grid-based [59] neural network:

$$(\mathbf{c}^s, \sigma^s) = \text{MLP}(\mathbf{G}_\theta^s(\text{contract}(\mathbf{x}), \mathbf{d}); f), \quad f = \mathbf{V}_{icv}^{t_i}(\mathbf{x}), \quad (4)$$

where $f = \mathbf{V}_{icv}^{t_i}(\mathbf{x})$ is the neural feature trilinearly interpolated from the collaborative geometry BEV volume $\mathbf{V}_{icv}^{t_i}$ at the location \mathbf{x} , $\mathbf{G}_\theta^s(\cdot, \cdot)$ is explicit multi-level hash grid representation with the generic f features for fast static collaborative neural field training. Meanwhile, owing to the collaborative scenarios are unbounded, we utilize $\text{contract}(\cdot)$ [51] to map 3D scenario position into a bounded ball of radius 2 with regularization, making the estimation optimization process faster and better. Hence, we can compute the color of the pixel (corresponding to the ray $\mathbf{r}(u_k)$ using numerical quadrature for approximating the collaborative volume rendering interval[64]:

$$\mathbf{C}^s(\mathbf{r}) = \sum_{k=1}^K T^s(u_k) \alpha^s(\sigma^s(u_k) \delta_k) \mathbf{c}^s(u_k), \quad (5a)$$

$$T^s(u_k) = \exp\left(-\sum_{k'=1}^{k-1} \sigma^s(u_k) \delta_k\right), \quad (5b)$$

where $\alpha^s(x) = 1 - \exp(-x)$ and $\delta_k = u_{k+1} - u_k$ is the distance between two quadrature points. The K quadrature points $\{u_k\}_{k=1}^K$ are drawn uniformly between u_n and u_f , which denotes the near and far of the bounded collaborative scenarios. $T^s(u_k)$ indicates the accumulated transmittance from u_n to u_k . Here, we denote \mathbf{r}_i as the rays passing through the pixel i . Then, the collaborative static neural loss \mathcal{L}_{static} is defined to minimize the l_2 -loss between the estimated colors $\mathbf{C}^s(\mathbf{r}_i)$ and the ground truth colors $\mathbf{C}^{gt}(\mathbf{r}_i)$ in the static regions (where $\mathbf{M}(\mathbf{r}_i) = 0$):

$$\mathcal{L}_{static} = \sum_i \|\mathbf{C}^s(\mathbf{r}_i) - \mathbf{C}^{gt}(\mathbf{r}_i) \cdot (1 - \mathbf{M}(\mathbf{r}_i))\|_2^2 \quad (6)$$

4.4 Dynamic Collaborative Neural Field

While the static collaborative neural field is being modeled, Step 2d is building the dynamic collaborative neural field to construct the foreground of camera views. Our dynamic collaborative neural field takes 4D spatiotemporal position features as input to model dynamic motion of 3D scene flow $\mathbf{s}_{fw}, \mathbf{s}_{bw}$, volume density $\sigma_{t_i}^d$, color $\mathbf{c}_{t_i}^d$ and blending weight \mathbf{b} (Note that blending weights learns how to blend the results from both the static and dynamic collaborative neural fields in an unsupervised manner, avoiding background’s structure and appearance conflict the moving objects.):

$$(\mathbf{s}_{fw}, \mathbf{s}_{bw}, \mathbf{c}_{t_i}^d, \sigma_{t_i}^d, \mathbf{b}) = \text{MLP}(\Delta(\mathbf{G}_\theta^d(\text{contract}(\mathbf{x}), \mathbf{d}), t_i); f), \quad f = \mathbf{V}_{icv}^{t_i}(\mathbf{x}), \quad (7)$$

where \mathbf{G}_θ^d shares the same hash grid representations, but for the dynamic collaborative neural field optimization; $\Delta(\cdot, \cdot)$ is the temporal interpolation functions, which makes the MLP can efficiently learn the features between keyframes in a scalable manner. Meanwhile, to improve the temporal consistency of the proposed field, we compute the collaborative scene flow neighbors $\mathbf{r}(u_k) + \mathbf{s}_{fw}$ and $\mathbf{r}(u_k) - \mathbf{s}_{bw}$ with the predicted collaborative scene flow $\mathbf{s}_{fw}, \mathbf{s}_{bw}$ to warp the collaborative neural field from the neighboring time instance to the current time. Hence, we can obtain the corresponding density and color of adjacent time by querying the same MLPs model at $\mathbf{r}(u_k) + \mathbf{s}$:

$$(\mathbf{c}_{t_i+1}^d, \sigma_{t_i+1}^d) = \text{MLP}(\Delta(\mathbf{G}_\theta^d(\text{contract}(\mathbf{x} + \mathbf{s}_{fw}), \mathbf{d}), t_i + 1)) \quad (8a)$$

$$(\mathbf{c}_{t_i-1}^d, \sigma_{t_i-1}^d) = \text{MLP}(\Delta(\mathbf{G}_\theta^d(\text{contract}(\mathbf{x} - \mathbf{s}_{bw}), \mathbf{d}), t_i - 1)) \quad (8b)$$

We can compute the color of a dynamic pixel of collaborative view at time t_i . Hence, with both the static and dynamic collaborative neural fields model, we can easily compose them into a complete model using the predicted blending weight \mathbf{b} and render full color $\mathbf{C}^{full}(\mathbf{r})$ frames at noisy views and time. We utilize the following approximate of collaborative volume rendering integral:

$$\mathbf{C}_{t_i}^{full}(\mathbf{r}) = \sum_{k=1}^K T_{t_i}^{full} (\alpha^d(\sigma_{t_i}^d \delta_k)(1 - \mathbf{b})\mathbf{c}_{t_i}^d + \alpha^s(\sigma^s \delta_k)\mathbf{b}\mathbf{c}^s) \quad (9)$$

Similar to the static collaborative rendering loss, we train the dynamic collaborative neural model by minimizing the l_2 reconstruction loss under time unit $\tau = \{t_i, t_i - 1, t_i + 1\}$:

$$\mathcal{L}_{dyn} = \sum_{t \in \tau} \sum_i \|(\mathbf{C}_t^{full}(\mathbf{r}_i) - \mathbf{C}^{gt}(\mathbf{r}_i))\|_2^2 \quad (10)$$

To reduce the amount of ambiguity caused by the sparse views during collaborative perception process, we construct motion matching loss to constrain the proposed dynamic collaborative neural field. As we do not have direct 3D supervision for predicted collaborative scene flow from the motion MLP model, we utilize 2D optical flow \mathbf{f} as indirect supervision. Specifically, we first use the estimated collaborative scene flow to obtain the corresponding 3D point. Then, we project these 3D points onto the 2D reference frame with $\varphi(\cdot)$ function. Hence, we can compute the projected collaborative scene optical flow and enforce it to match the estimated optical flow as follows:

$$\mathcal{L}_{opt} = \sum_i \left(\varphi(\mathbf{s}_{\{bw, fw\}}(\mathbf{r}_i)) - \mathbf{f}_{\{bw, fw\}}^{gt}(\mathbf{r}_i) \right) \quad (11)$$

Meanwhile, we also regularize the consistency of the collaborative scene flow by minimizing the cycle consistency loss \mathcal{L}_{cyc} . See more details in the Appendix B.6.

Table 1: Map-view segmentation of different baseline methods *w.o/w* the proposed RCDN on the OPV2V-N camera-track with one random noisy camera failure in the testing phase. We report IoU for all classes.

Model / Metric	Static Part (<i>Perf. Comparison</i>)				Dynamic Part Vehicle	
	Drivable Area		Lane		Normal	Failure
	Normal	Failure	Normal	Failure		
		<i>w.o/w</i> RCDN		<i>w.o/w</i> RCDN		
F-Cooper[1]	45.44	28.87/44.89(↑55.49%)	33.17	15.95/32.23(↑102.07%)	63.33	29.70/61.76(↑107.95%)
AttFuse[16]	45.59	27.99/44.38(↑58.56%)	33.76	18.77/31.50(↑67.82%)	54.14	24.76/52.15(↑110.62%)
DiscoNet[42]	42.30	24.31/38.54(↑58.54%)	24.24	12.29/22.97(↑86.90%)	46.56	9.25/43.03(↑365.19%)
V2VNet[35]	41.70	27.99/39.72(↑41.91%)	27.14	10.52/25.24(↑139.92%)	42.57	11.28/42.76(↑279.08%)
CoBEVT[6]	51.96	32.08/47.19(↑47.10%)	34.19	14.45/29.55(↑104.50%)	56.61	32.41/55.10(↑70.01%)

4.5 Training Details and Optimization

To train the overall system, we supervise two tasks: static and dynamic collaborative neural fields, respectively. Meanwhile, during the training process, the static collaborative field and dynamic collaborative field are trained separately. The total reconstruction loss is a weighted combination as the following:

$$\mathcal{L}_{total} = \lambda_1 \mathcal{L}_{static} + \lambda_2 \mathcal{L}_{dyn} + \lambda_3 \mathcal{L}_{opt} + \lambda_4 \mathcal{L}_{cyc} \quad (12)$$

5 Experimental Results

We create the first camera-insensitivity collaborative perception dataset and conduct extensive experiments on OPV2V-N. To ensure the consistency of the input noisy camera data and verify the effectiveness of RCDN, we set the noisy camera data to be in the failed situation[27]. Meanwhile, the task of the experiments is map segmentation, including the performance of the vehicle, drivable area (Dr. area) and lane, totaling three classes. We utilize the Intersection over Union (IoU) between map prediction and ground truth map-view labels as the performance metric.

5.1 Datasets

OPV2V-N. To facilitate research on camera-insensitivity for collaborative perception, we propose a simulation dataset dubbed OPV2V-N. In OPV2V dataset, there is a lack of mask labels for distinguishing between foreground and background views, as well as optical flow labels for supervising the scene flow. For this purpose, we collect more data to bridge the gap between neural field and collaborative perception, leading to the new OPV2V-N datasets. Specifically, we utilize the OneFormer[65] detector to extract the foreground mask labels and mainstream RAFT[66] detector to compute the optical flow between image pairs. Meanwhile, we manually annotate which part of the performance degradation is triggered by camera failure in different scenarios. See more details in the Appendix A.

5.2 Quantitative Evaluation

Benchmark comparison. The baseline methods include F-Cooper[1], AttFuse[16], DiscoNet[42], V2VNet[35] and CoBEVT[6]. All methods use the same BEV feature encoder based on CVT[67]. To validate the portability of the RCDN, we compare different baseline methods *w.o/w* RCDN under unpredictable camera failure settings. Table 1 shows that the map-view segmentation performance of different baseline methods *w.o/w* the proposed RCDN with only one number random noisy camera failure in the testing phase on the OPV2V-N dataset. We see that i) for static part, each baseline method with one camera failure drops about 37.73%/42.54%/32.87% (*Avg/Max/Min*) and 52.93%/61.25%/44.40% for drivable area and lane, respectively. However, each baseline method *w.* RCDN under the same camera failure situation only decreases about 5.34%/9.17%/1.22% and 7.08%/13.59%/2.85%, respectively. Compared to the *w.o* RCDN baseline methods, RCDN can improve the performance of drivable area and lane for 52.32%/58.54%/47.10% and 100.37%/139.92%/67.82%, respectively; ii) compared to the static part, as we all know, the fusion stage in collaborative perception process needs more effort on the multi-view based BEV feature map to highlight the corresponding dynamic part. Hence, the

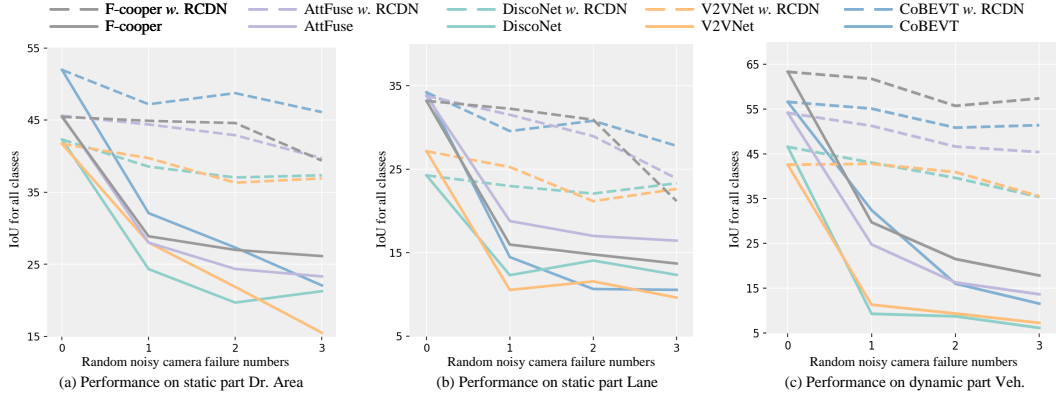


Figure 3: Comparison of the performance of other baseline methods *w.o/w* the proposed RCDN under the random noisy (failed situation) camera numbers from 0 to 3. RCDN can be ported to other baseline methods and stabilize the performance under different level camera failure situations on OPV2V-N dataset.

Table 2: Ablation Study on OPV2V-N dataset.

Modules		Dr. Area	Lanes	Dynamic Veh.
Neural Field	Time Model			
✗	✗	24.55	10.07	30.67
✓	✗	24.47	11.71	41.55
✓	✓	27.37	10.63	46.65

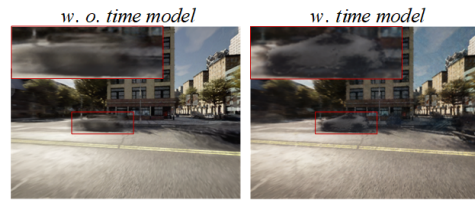


Figure 4: Effectiveness of dynamic neural field.

baseline methods’ dynamic performance suffers more from camera failure than the static part, causing about a 60.75%/42.72%/80.14% performance drop. Nevertheless, RCDN also demonstrates robustness to the dynamic foreground object modeling, with only a 3.31%/7.58%/0.47% performance decrease for the dynamic part, improving the *w.o* RCDN baseline methods’ performance by 186.57%/365.19%/70.01%. Meanwhile, as for the communication cost, similar to [42], we only utilize the C^{gt} labels during the training stage, meaning we leave the communication burden to the training stage and do not introduce extra information during the inference.

Robust to extremely noisy camera data. We conduct experiments to validate the performance under the impact of random noisy camera numbers. Figure 3 shows the map-view segmentation performance of the different baselines methods *w.o/w* the proposed RCDN under varying levels of camera failures situation on OPV2V-N, where the x -axis is the expectation of the number of random failed cameras during the inference stage and y -axis is the segmentation performance. Note that, when the x -axis is at 0, it represents standard collaborative perception without any camera failures. We see that i) the proposed RCDN can stabilize all the baseline methods in both static and dynamic part of map-view segmentation performance at all camera failure settings; ii) as for the static part, with the RCDN can maintain the 87.84%/88.72%/86.64% Dr. area performance of the standard setting even under three random failed views during the collaboration process, compared with the *w.o.* RCDN only about 47.68%/57.48%/37.15%. Note that the V2VNet baseline method’s performance degrades sharply as the failed camera number increases, however, with RCDN, the V2VNet can settle in a considerable performance even with the failed camera number increases; iii) as for the dynamic part, some baseline methods are crashed even with only one random camera failure situation, *e.g.* DiscoNet only maintains about 19.87% performance of the standard collaborative perception setting, and almost every baseline method is unusable when there are three random camera failures, only about 20.73%/28.11%/13.09% of the standard situation. Nevertheless, with the RCDN, we see that all baseline methods still perform well even when three random failed camera situation appear, maintaining the 84.95%/90.81%/75.93% dynamic performance of the standard situation.

5.3 Qualitative Evaluation

Visualization of segmentation. We illustrate the map-view segmentation of other baseline methods *w.o/w* RCDN and the corresponding repaired camera view in Figure 5. The random camera failure number is one. The orange represents the drivable area, the blue represents the lanes and the teal

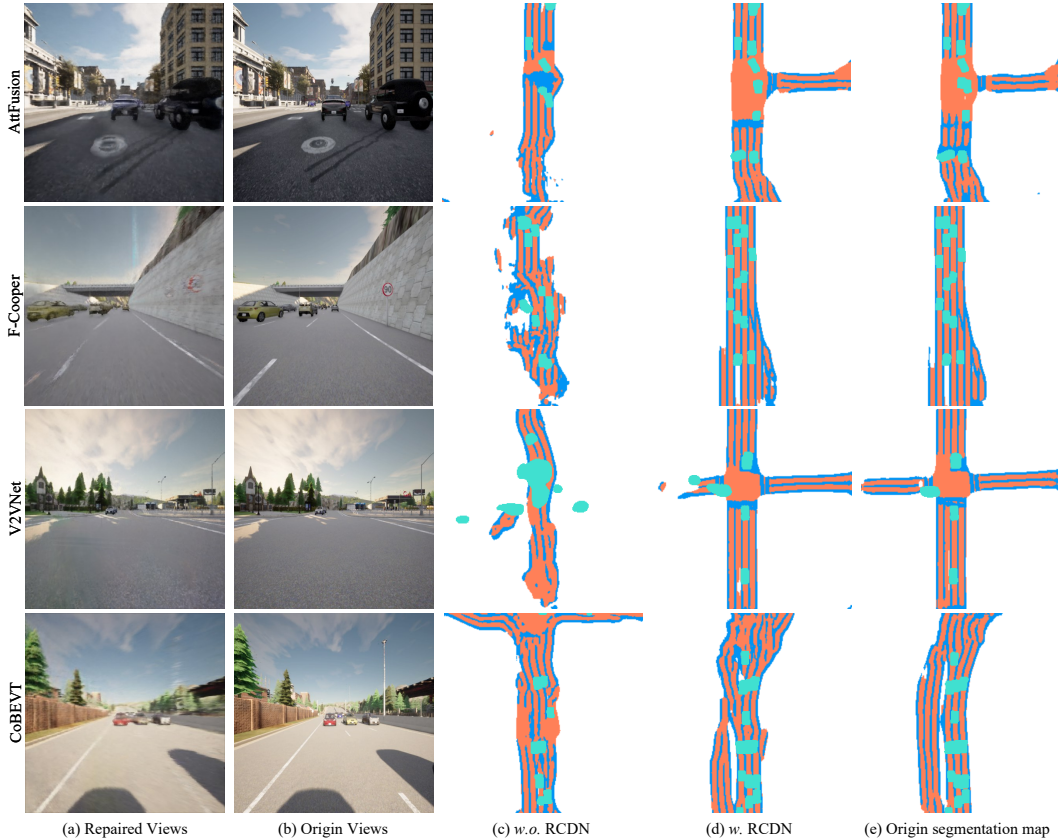


Figure 5: Visualization of different baseline methods w. RCDN with one random camera failure.

represents the vehicles. We can see that i) other baseline methods show significant improvement in w. RCDN under noisy camera data; ii) V2VNet that collapses with noise camera data can also achieve the same level of performance as the origin data with the help of RCDN.

5.4 Ablation Study

We conduct ablation studies on OPV2V-N with the CoBEVT baseline method. Table 2 assesses the effectiveness of the proposed two field phases. We see that i) only one neural field can recover most static part performance from the noisy camera data; ii) the proposed time model in collaborative dynamic fields can handle the motion blurry caused by the vehicles, shown in Figure 4. Meanwhile, we compare the training efficiency of the proposed RCDN with existing dynamic fields modeling methods[68], as illustrated in Figure 6. Our approach, which leverages explicit grid and geometry feature-based representations, accelerates the training process by approximately $24\times$ compared to the existing implicit MLP-based modeling, while also achieving superior PSNR quality. See more discussions in the Appendix B.2.

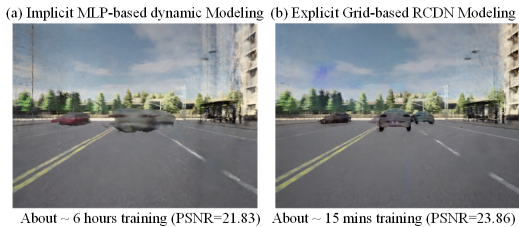


Figure 6: Comparison between existing dynamic field modeling and the proposed RCDN.

6 Conclusion and Limitation

We formulate the camera-insensitivity collaborative perception task, which considers harsh realities of real-world sensors that may cause unpredictable random camera failures during collaborative communication. We further propose RCDN, a robust camera-insensitivity collaborative perception with a novel dynamic feature-based 3D neural modeling. The core idea of RCDN is to construct collaborative neural rendering field representations to recover failed perceptual messages sent by

multiple agents. Comprehensive experiments show that RCDN can be portable to other baseline methods and stabilize the performance with a considerable level under all settings and far superior robustness with random camera failures.

Limitation and future work. The current work focuses on addressing the camera-insensitivity problem in collaborative perception. It is evident that accurate reconstruction can compensate for the negative impact of noisy camera features on collaborative perception. In the future, we expect more works on exploring real-time collaborative neural field modeling with 3D Gaussian splatting.

References

- [1] Qi Chen, Xu Ma, Sihai Tang, Jingda Guo, Qing Yang, and Song Fu. F-cooper: Feature based cooperative perception for autonomous vehicle edge computing system using 3d point clouds. In *Proceedings of the 4th ACM/IEEE Symposium on Edge Computing*, pages 88–100, 2019.
- [2] Runsheng Xu, Yi Guo, Xu Han, Xin Xia, Hao Xiang, and Jiaqi Ma. Openca: an open cooperative driving automation framework integrated with co-simulation. In *2021 IEEE International Intelligent Transportation Systems Conference (ITSC)*, pages 1155–1162. IEEE, 2021.
- [3] Yiming Li, Dekun Ma, Ziyang An, Zixun Wang, Yiqi Zhong, Siheng Chen, and Chen Feng. V2x-sim: Multi-agent collaborative perception dataset and benchmark for autonomous driving. *IEEE Robotics and Automation Letters*, 7(4):10914–10921, 2022.
- [4] James Tu, Tsunhsuan Wang, Jingkang Wang, Sivabalan Manivasagam, Mengye Ren, and Raquel Urtasun. Adversarial attacks on multi-agent communication. In *Proceedings of the IEEE/CVF International Conference on Computer Vision*, pages 7768–7777, 2021.
- [5] Jiaxun Cui, Hang Qiu, Dian Chen, Peter Stone, and Yuke Zhu. Coopernaut: End-to-end driving with cooperative perception for networked vehicles. In *Proceedings of the IEEE/CVF Conference on Computer Vision and Pattern Recognition*, pages 17252–17262, 2022.
- [6] Runsheng Xu, Zhengzhong Tu, Hao Xiang, Wei Shao, Bolei Zhou, and Jiaqi Ma. Cobevt: Cooperative bird’s eye view semantic segmentation with sparse transformers. 2022.
- [7] Hao Xiang, Runsheng Xu, and Jiaqi Ma. Hm-vit: Hetero-modal vehicle-to-vehicle cooperative perception with vision transformer. *arXiv preprint arXiv:2304.10628*, 2023.
- [8] Ebtehal Turki Alotaibi, Shahad Saleh Alqefari, and Anis Koubaa. Lsar: Multi-uav collaboration for search and rescue missions. *IEEE Access*, 7:55817–55832, 2019.
- [9] Jürgen Scherer, Saeed Yahyanejad, Samira Hayat, Evsen Yanmaz, Torsten Andre, Asif Khan, Vladimir Vukadinovic, Christian Bettstetter, Hermann Hellwagner, and Bernhard Rinner. An autonomous multi-uav system for search and rescue. In *Proceedings of the First Workshop on Micro Aerial Vehicle Networks, Systems, and Applications for Civilian Use*, page 33–38, New York, NY, USA, 2015.
- [10] Yue Hu, Shaoheng Fang, Weidi Xie, and Siheng Chen. Aerial monocular 3d object detection. *IEEE Robotics and Automation Letters*, 8(4):1959–1966, 2023.
- [11] Lukas Bernreiter, Shehryar Khattak, Lionel Ott, Roland Siegwart, Marco Hutter, and Cesar Cadena. A framework for collaborative multi-robot mapping using spectral graph wavelets. *The International Journal of Robotics Research*, 0(0):02783649241246847, 0.
- [12] Luiz Eugênio Santos Araújo Filho and Cairo Lúcio Nascimento Júnior. Multi-robot autonomous exploration and map merging in unknown environments. In *2022 IEEE International Systems Conference (SysCon)*, pages 1–8, 2022.
- [13] Yiming Li, Juexiao Zhang, Dekun Ma, Yue Wang, and Chen Feng. Multi-robot scene completion: Towards task-agnostic collaborative perception. In *6th Annual Conference on Robot Learning*, 2022.
- [14] Runsheng Xu, Xin Xia, Jinlong Li, Hanzhao Li, Shuo Zhang, Zhengzhong Tu, Zonglin Meng, Hao Xiang, Xiaoyu Dong, Rui Song, et al. V2v4real: A real-world large-scale dataset for vehicle-to-vehicle cooperative perception. In *Proceedings of the IEEE/CVF Conference on Computer Vision and Pattern Recognition*, pages 13712–13722, 2023.
- [15] Haibao Yu, Yizhen Luo, Mao Shu, Yiyi Huo, Zebang Yang, Yifeng Shi, Zhenglong Guo, Hanyu Li, Xing Hu, Jirui Yuan, et al. Dair-v2x: A large-scale dataset for vehicle-infrastructure cooperative 3d object detection. In *Proceedings of the IEEE/CVF Conference on Computer Vision and Pattern Recognition*, pages 21361–21370, 2022.

- [16] Runsheng Xu, Hao Xiang, Xin Xia, Xu Han, Jinlong Li, and Jiaqi Ma. Opv2v: An open benchmark dataset and fusion pipeline for perception with vehicle-to-vehicle communication. In *2022 International Conference on Robotics and Automation (ICRA)*, pages 2583–2589. IEEE, 2022.
- [17] Walter Zimmer, Gerhard Arya Wardana, Suren Sritharan, Xingcheng Zhou, Rui Song, and Alois C. Knoll. Tumtraf v2x cooperative perception dataset. In *2024 IEEE/CVF International Conference on Computer Vision and Pattern Recognition (CVPR)*. IEEE/CVF, 2024.
- [18] Runsheng Xu, Jinlong Li, Xiaoyu Dong, Hongkai Yu, and Jiaqi Ma. Bridging the domain gap for multi-agent perception. *arXiv preprint arXiv:2210.08451*, 2022.
- [19] Yunsheng Ma, Juanwu Lu, Can Cui, Sicheng Zhao, Xu Cao, Wenqian Ye, and Ziran Wang. Macp: Efficient model adaptation for cooperative perception. In *Proceedings of the IEEE/CVF Winter Conference on Applications of Computer Vision*, pages 3373–3382, 2024.
- [20] Yiming Li, Qi Fang, Jiamu Bai, Siheng Chen, Felix Juefei-Xu, and Chen Feng. Among us: Adversarially robust collaborative perception by consensus. In *Proceedings of the IEEE/CVF International Conference on Computer Vision (ICCV)*, pages 186–195, October 2023.
- [21] James Tu, Tsunhsuan Wang, Jingkang Wang, Sivabalan Manivasagam, Mengye Ren, and Raquel Urtasun. Adversarial attacks on multi-agent communication. In *2021 IEEE/CVF International Conference on Computer Vision (ICCV)*, pages 7748–7757, 2021.
- [22] Francesco Secci and Andrea Ceccarelli. On failures of rgb cameras and their effects in autonomous driving applications. In *2020 IEEE 31st International Symposium on Software Reliability Engineering (ISSRE)*, pages 13–24, 2020.
- [23] Kui Ren, Qian Wang, Cong Wang, Zhan Qin, and Xiaodong Lin. The security of autonomous driving: Threats, defenses, and future directions. *Proceedings of the IEEE*, 108(2):357–372, 2020.
- [24] Rui Song, Chenwei Liang, Hu Cao, Zhiran Yan, Walter Zimmer, Markus Gross, Andreas Festag, and Alois Knoll. Collaborative semantic occupancy prediction with hybrid feature fusion in connected automated vehicles. 2024.
- [25] Xiang Li, Junbo Yin, Wei Li, Chengzhong Xu, Ruigang Yang, and Jianbing Shen. Di-v2x: Learning domain-invariant representation for vehicle-infrastructure collaborative 3d object detection. *Proceedings of the AAAI Conference on Artificial Intelligence*, 38(4):3208–3215, Mar. 2024.
- [26] Hao Xiang, Runsheng Xu, Xin Xia, Zhaoliang Zheng, Bolei Zhou, and Jiaqi Ma. V2xp-asm: Generating adversarial scenes for vehicle-to-everything perception. In *2023 IEEE International Conference on Robotics and Automation (ICRA)*, pages 3584–3591, 2023.
- [27] Kaicheng Yu, Tang Tao, Hongwei Xie, Zhiwei Lin, Tingting Liang, Bing Wang, Peng Chen, Dayang Hao, Yongtao Wang, and Xiaodan Liang. Benchmarking the robustness of lidar-camera fusion for 3d object detection. In *2023 IEEE/CVF Conference on Computer Vision and Pattern Recognition Workshops (CVPRW)*, pages 3188–3198, 2023.
- [28] Youngseok Kim, Juyeb Shin, Sanmin Kim, In-Jae Lee, Jun Won Choi, and Dongsuk Kum. Crn: Camera radar net for accurate, robust, efficient 3d perception. In *Proceedings of the IEEE/CVF International Conference on Computer Vision (ICCV)*, pages 17615–17626, October 2023.
- [29] Xuyang Bai, Zeyu Hu, Xinge Zhu, Qingqiu Huang, Yilun Chen, Hongbo Fu, and Chiew-Lan Tai. Transfusion: Robust lidar-camera fusion for 3d object detection with transformers. In *Proceedings of the IEEE/CVF Conference on Computer Vision and Pattern Recognition (CVPR)*, pages 1090–1099, June 2022.
- [30] Tingting Liang, Hongwei Xie, Kaicheng Yu, Zhongyu Xia, Zhiwei Lin, Yongtao Wang, Tao Tang, Bing Wang, and Zhi Tang. Bevfusion: A simple and robust lidar-camera fusion framework. In S. Koyejo, S. Mohamed, A. Agarwal, D. Belgrave, K. Cho, and A. Oh, editors, *Advances in Neural Information Processing Systems*, volume 35, pages 10421–10434. Curran Associates, Inc., 2022.
- [31] Vishwanath A. Sindagi, Yin Zhou, and Oncel Tuzel. Mvx-net: Multimodal voxelnet for 3d object detection. In *2019 International Conference on Robotics and Automation (ICRA)*, pages 7276–7282, 2019.
- [32] Yue Wang, Vitor Campagnolo Guizilini, Tianyuan Zhang, Yilun Wang, Hang Zhao, and Justin Solomon. Detr3d: 3d object detection from multi-view images via 3d-to-2d queries. In Aleksandra Faust, David Hsu, and Gerhard Neumann, editors, *Proceedings of the 5th Conference on Robot Learning*, volume 164 of *Proceedings of Machine Learning Research*, pages 180–191. PMLR, 08–11 Nov 2022.

- [33] Yin Zhou and Oncel Tuzel. Voxelnet: End-to-end learning for point cloud based 3d object detection. In *Proceedings of the IEEE conference on computer vision and pattern recognition*, pages 4490–4499, 2018.
- [34] Maria Christopoulou, Sokratis Barmponakis, Harilaos Koumaras, and Alexandros Kalokylos. Artificial intelligence and machine learning as key enablers for v2x communications: A comprehensive survey. *Vehicular Communications*, 39:100569, 2023.
- [35] Tsun-Hsuan Wang, Sivabalan Manivasagam, Ming Liang, Bin Yang, Wenyuan Zeng, and Raquel Urtasun. V2vnet: Vehicle-to-vehicle communication for joint perception and prediction. In *Proceedings of the European Conference on Computer Vision (ECCV)*, pages 605–621, 2020.
- [36] Yifan Lu, Yue Hu, Yiqi Zhong, Dequan Wang, Siheng Chen, and Yanfeng Wang. An extensible framework for open heterogeneous collaborative perception. In *The Twelfth International Conference on Learning Representations*, 2024.
- [37] Yue Hu, Yifan Lu, Runsheng Xu, Weidi Xie, Siheng Chen, and Yanfeng Wang. Collaboration helps camera overtake lidar in 3d detection. In *Proceedings of the IEEE/CVF Conference on Computer Vision and Pattern Recognition*, pages 9243–9252, 2023.
- [38] Yen-Cheng Liu, Junjiao Tian, Chih-Yao Ma, Nathan Glaser, Chia-Wen Kuo, and Zsolt Kira. Who2com: Collaborative perception via learnable handshake communication. In *2020 IEEE International Conference on Robotics and Automation (ICRA)*, pages 6876–6883, 2020.
- [39] Yen-Cheng Liu, Junjiao Tian, Nathaniel Glaser, and Zsolt Kira. When2com: multi-agent perception via communication graph grouping. In *Proceedings of the IEEE/CVF Conference on Computer Vision and Pattern Recognition*, pages 4106–4115, 2020.
- [40] Yue Hu, Shaoheng Fang, Zixing Lei, Yiqi Zhong, and Siheng Chen. Where2comm: Communication-efficient collaborative perception via spatial confidence maps. *Advances in neural information processing systems*, 35:4874–4886, 2022.
- [41] Tianhang Wang, Guang Chen, Kai Chen, Zhengfa Liu, Bo Zhang, Alois Knoll, and Changjun Jiang. Umc: A unified bandwidth-efficient and multi-resolution based collaborative perception framework. In *2023 IEEE/CVF International Conference on Computer Vision (ICCV)*, pages 8153–8162, 2023.
- [42] Yiming Li, Shunli Ren, Pengxiang Wu, Siheng Chen, Chen Feng, and Wenjun Zhang. Learning distilled collaboration graph for multi-agent perception. *Advances in Neural Information Processing Systems*, 34:29541–29552, 2021.
- [43] Runsheng Xu, Hao Xiang, Zhengzhong Tu, Xin Xia, Ming-Hsuan Yang, and Jiaqi Ma. V2x-vit: Vehicle-to-everything cooperative perception with vision transformer. *ArXiv*, abs/2203.10638, 2022.
- [44] Nicholas Vadivelu, Mengye Ren, James Tu, Jingkang Wang, and Raquel Urtasun. Learning to communicate and correct pose errors. In *4th Conference on Robot Learning (CoRL)*, 2020.
- [45] Yifan Lu, Quanhao Li, Baoan Liu, Mehrdad Dianati, Chen Feng, Siheng Chen, and Yanfeng Wang. Robust collaborative 3d object detection in presence of pose errors. In *2023 IEEE International Conference on Robotics and Automation (ICRA)*, pages 4812–4818. IEEE, 2023.
- [46] Zixing Lei, Shunli Ren, Yue Hu, Wenjun Zhang, and Siheng Chen. Latency-aware collaborative perception. In *Computer Vision–ECCV 2022: 17th European Conference, Tel Aviv, Israel, October 23–27, 2022, Proceedings, Part XXXII*, pages 316–332. Springer, 2022.
- [47] Sizhe Wei, Yuxi Wei, Yue Hu, Yifan Lu, Yiqi Zhong, Siheng Chen, and Ya Zhang. Asynchrony-robust collaborative perception via bird’s eye view flow. In *Advances in Neural Information Processing Systems*, 2023.
- [48] Dian Chen and Philipp Krähenbühl. Learning from all vehicles. In *Proceedings of the IEEE/CVF Conference on Computer Vision and Pattern Recognition*, pages 17222–17231, 2022.
- [49] Ruizhao Zhu, Peng Huang, Eshed Ohn-Bar, and Venkatesh Saligrama. Learning to drive anywhere. In *7th Annual Conference on Robot Learning*, 2023.
- [50] Ben Mildenhall, Pratul P. Srinivasan, Matthew Tancik, Jonathan T. Barron, Ravi Ramamoorthi, and Ren Ng. Nerf: Representing scenes as neural radiance fields for view synthesis. In *ECCV*, 2020.
- [51] Jonathan T Barron, Ben Mildenhall, Dor Verbin, Pratul P Srinivasan, and Peter Hedman. Mip-nerf 360: Unbounded anti-aliased neural radiance fields. In *Proceedings of the IEEE/CVF Conference on Computer Vision and Pattern Recognition*, pages 5470–5479, 2022.

- [52] Jonathan T Barron, Ben Mildenhall, Dor Verbin, Pratul P Srinivasan, and Peter Hedman. Zip-nerf: Anti-aliased grid-based neural radiance fields. In *Proceedings of the IEEE/CVF International Conference on Computer Vision*, pages 19697–19705, 2023.
- [53] Wenbo Hu, Yuling Wang, Lin Ma, Bangbang Yang, Lin Gao, Xiao Liu, and Yuewen Ma. Tri-miprf: Tri-mip representation for efficient anti-aliasing neural radiance fields. In *Proceedings of the IEEE/CVF International Conference on Computer Vision*, pages 19774–19783, 2023.
- [54] Sara Fridovich-Keil, Alex Yu, Matthew Tancik, Qinhong Chen, Benjamin Recht, and Angjoo Kanazawa. Plenoxels: Radiance fields without neural networks. In *Proceedings of the IEEE/CVF Conference on Computer Vision and Pattern Recognition*, pages 5501–5510, 2022.
- [55] Cheng Sun, Min Sun, and Hwann-Tzong Chen. Direct voxel grid optimization: Super-fast convergence for radiance fields reconstruction. In *Proceedings of the IEEE/CVF Conference on Computer Vision and Pattern Recognition*, pages 5459–5469, 2022.
- [56] Haiyan Jin, Isabella Liu, Peijia Xu, Xiaoshuai Zhang, Songfang Han, Sai Bi, Xiaowei Zhou, Zexiang Xu, and Hao Su. Tensor: Tensorial inverse rendering. In *Proceedings of the IEEE/CVF Conference on Computer Vision and Pattern Recognition*, pages 165–174, 2023.
- [57] Bernhard Kerbl, Georgios Kopanas, Thomas Leimkühler, and George Drettakis. 3d gaussian splatting for real-time radiance field rendering. *ACM Transactions on Graphics*, 42(4):1–14, 2023.
- [58] Jonathan T Barron, Ben Mildenhall, Matthew Tancik, Peter Hedman, Ricardo Martin-Brualla, and Pratul P Srinivasan. Mip-nerf: A multiscale representation for anti-aliasing neural radiance fields. In *Proceedings of the IEEE/CVF International Conference on Computer Vision*, pages 5855–5864, 2021.
- [59] Thomas Müller, Alex Evans, Christoph Schied, and Alexander Keller. Instant neural graphics primitives with a multiresolution hash encoding. *ACM transactions on graphics (TOG)*, 41(4):1–15, 2022.
- [60] Konstantinos Rematas, Andrew Liu, Pratul P Srinivasan, Jonathan T Barron, Andrea Tagliasacchi, Thomas Funkhouser, and Vittorio Ferrari. Urban radiance fields. In *Proceedings of the IEEE/CVF Conference on Computer Vision and Pattern Recognition*, pages 12932–12942, 2022.
- [61] Fan Lu, Yan Xu, Guang Chen, Hongsheng Li, Kwan-Yee Lin, and Changjun Jiang. Urban radiance field representation with deformable neural mesh primitives. In *Proceedings of the IEEE/CVF International Conference on Computer Vision*, pages 465–476, 2023.
- [62] Fan Lu, Kwan-Yee Lin, Yan Xu, Hongsheng Li, Guang Chen, and Changjun Jiang. Urban architect: Steerable 3d urban scene generation with layout prior. *arXiv preprint arXiv:2404.06780*, 2024.
- [63] Anpei Chen, Zexiang Xu, Fuqiang Zhao, Xiaoshuai Zhang, Fanbo Xiang, Jingyi Yu, and Hao Su. Mvsnerf: Fast generalizable radiance field reconstruction from multi-view stereo. *Proceedings of the IEEE/CVF International Conference on Computer Vision (ICCV)*, 2021.
- [64] Robert A Drebin, Loren Carpenter, and Pat Hanrahan. Volume rendering. *ACM Siggraph Computer Graphics*, 22(4):65–74, 1988.
- [65] Jitesh Jain, Jiachen Li, MangTik Chiu, Ali Hassani, Nikita Orlov, and Humphrey Shi. OneFormer: One Transformer to Rule Universal Image Segmentation. 2023.
- [66] Zachary Teed and Jia Deng. Raft: Recurrent all-pairs field transforms for optical flow. In *Computer Vision–ECCV 2020: 16th European Conference, Glasgow, UK, August 23–28, 2020, Proceedings, Part II 16*, pages 402–419. Springer, 2020.
- [67] Brady Zhou and Philipp Krähenbühl. Cross-view transformers for real-time map-view semantic segmentation. In *2022 IEEE/CVF Conference on Computer Vision and Pattern Recognition (CVPR)*, pages 13750–13759, 2022.
- [68] Chen Gao, Ayush Saraf, Johannes Kopf, and Jia-Bin Huang. Dynamic view synthesis from dynamic monocular video. In *Proceedings of the IEEE International Conference on Computer Vision*, 2021.
- [69] A. Schmied, T. Fischer, M. Danelljan, M. Pollefeys, and F. Yu. R3d3: Dense 3d reconstruction of dynamic scenes from multiple cameras. In *2023 IEEE/CVF International Conference on Computer Vision (ICCV)*, pages 3193–3203, Los Alamitos, CA, USA, oct 2023. IEEE Computer Society.
- [70] Diederik P Kingma and Jimmy Ba. Adam: A method for stochastic optimization. *arXiv preprint arXiv:1412.6980*, 2014.

- [71] Sanqing Qu, Tianpei Zou, Florian Röhrbein, Cewu Lu, Guang Chen, Dacheng Tao, and Changjun Jiang. Upcycling models under domain and category shift. In *CVPR*, 2023.
- [72] Anuroop Gaddam, Tim Wilkin, and Maia Angelova. Anomaly detection models for detecting sensor faults and outliers in the iot - a survey. In *2019 13th International Conference on Sensing Technology (ICST)*, pages 1–6, 2019.
- [73] Tianhang Wang, Kai Chen, Guang Chen, Bin Li, Zhijun Li, Zhengfa Liu, and Changjun Jiang. Gsc: A graph and spatio-temporal continuity based framework for accident anticipation. *IEEE Transactions on Intelligent Vehicles*, 9(1):2249–2261, 2024.

A OPV2V-N

To facilitate the research on camera-insensitivity for collaborative perception: i) firstly, as we discussed in related works, multi-view based collaborative perception heals the ill-posed of recovering noisy camera images just from single-view. Owing there are no labels of multi-view based overlap regions in existing collaborative perception, we manually collect the multi-view based overlap regions for RCDN experiments, shown in Figure 7. In detail, we will record the corresponding vehicle IDs, camera IDs and duration time t_{start}, t_{end} of the multi-view based overlap regions; ii) secondly, as we need to distinguish the foreground and background for static and dynamic collaborative neural fields, respectively. We extend the OPV2V[16] with more data format, such as the optical flow (supervise the $s_{fw,bw}$), mask labels, to bridge the gap between neural field and collaborative perception, as shown in Figure 8.

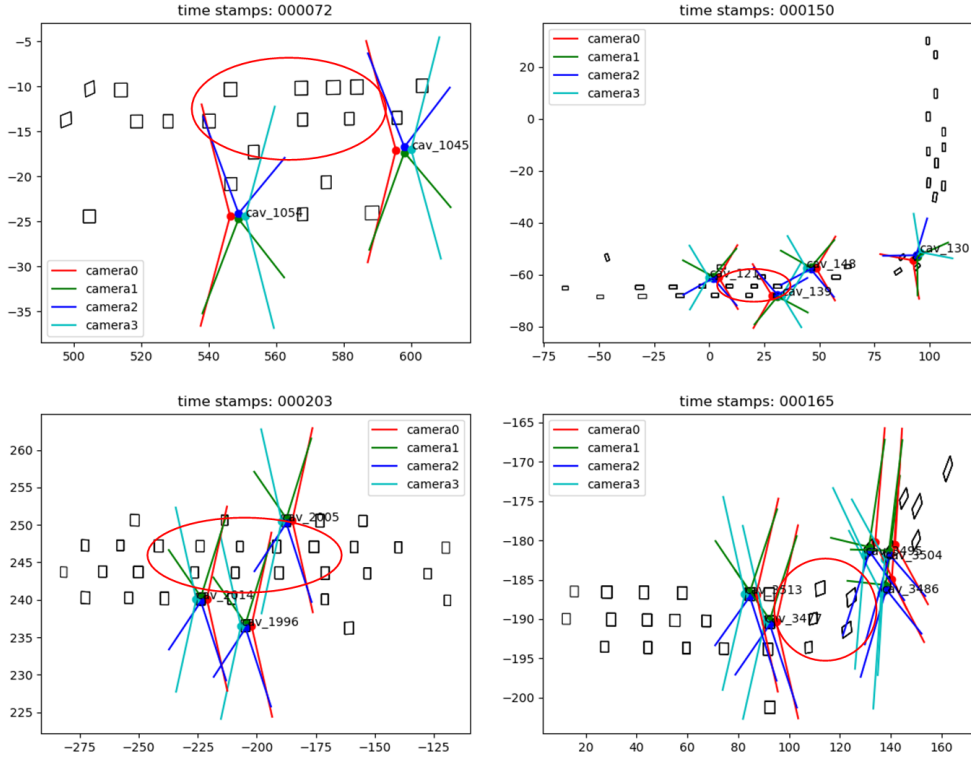


Figure 7: Visualization of manually labeling mechanisms. Note that the red circles represent the multi-view based overlap regions that are suitable for the random noisy situation. We will record the corresponding vehicle IDs, camera IDs and duration t_{start}, t_{end} of the overlap regions.

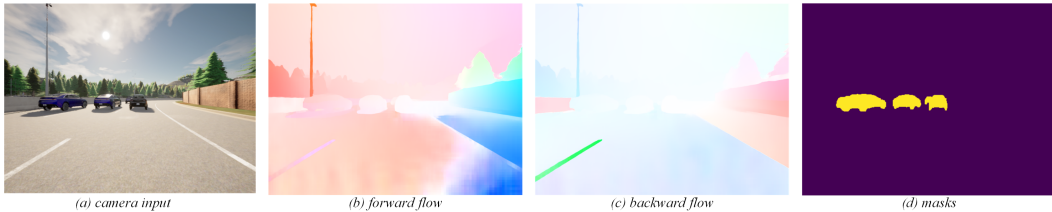


Figure 8: Visualization of extra data format.

Data analysis. We manually annotate about 65 scenes, which consists of a total of 6138 collaborative samples. Figure 10 presents some statistical analysis results regarding the OPV2V-N dataset. The OPV2V-N covers situations about 61.86%, 33.47%, and 4.66% for two, three, and four V2X collaborative agents, respectively. Meanwhile, before we conduct the corresponding RCDN experiments, we validate whether the random noisy camera data will affect the collaborative perception system. Table 3 shows that i) the noise actually degrades the system performance; ii) compared to static scenes,

dynamic vehicles are more susceptible to the influence of noisy data. With this prior knowledge, we decided to explore the RCDN algorithms and need to pay more attention to optimizing the design for dynamic vehicle perception. We also visualize the specific degradation caused by the noisy camera data, shown in Figure 9. Note that Figure 9 (a) degradation with missed vehicle inspections; Figure 9 (b) degradation with missed Dr. area and lane inspections; Figure 9 (c) degradation with both missed vehicle and Dr. area, lane inspections; Figure 9 (d) no degradation. Also, to make sure that the random noisy camera data is always inputted the same way and that performance does not change because of the different types of noise, like blurred or occluded, we replace the manually annotated camera IDs under the camera failure situation[27].

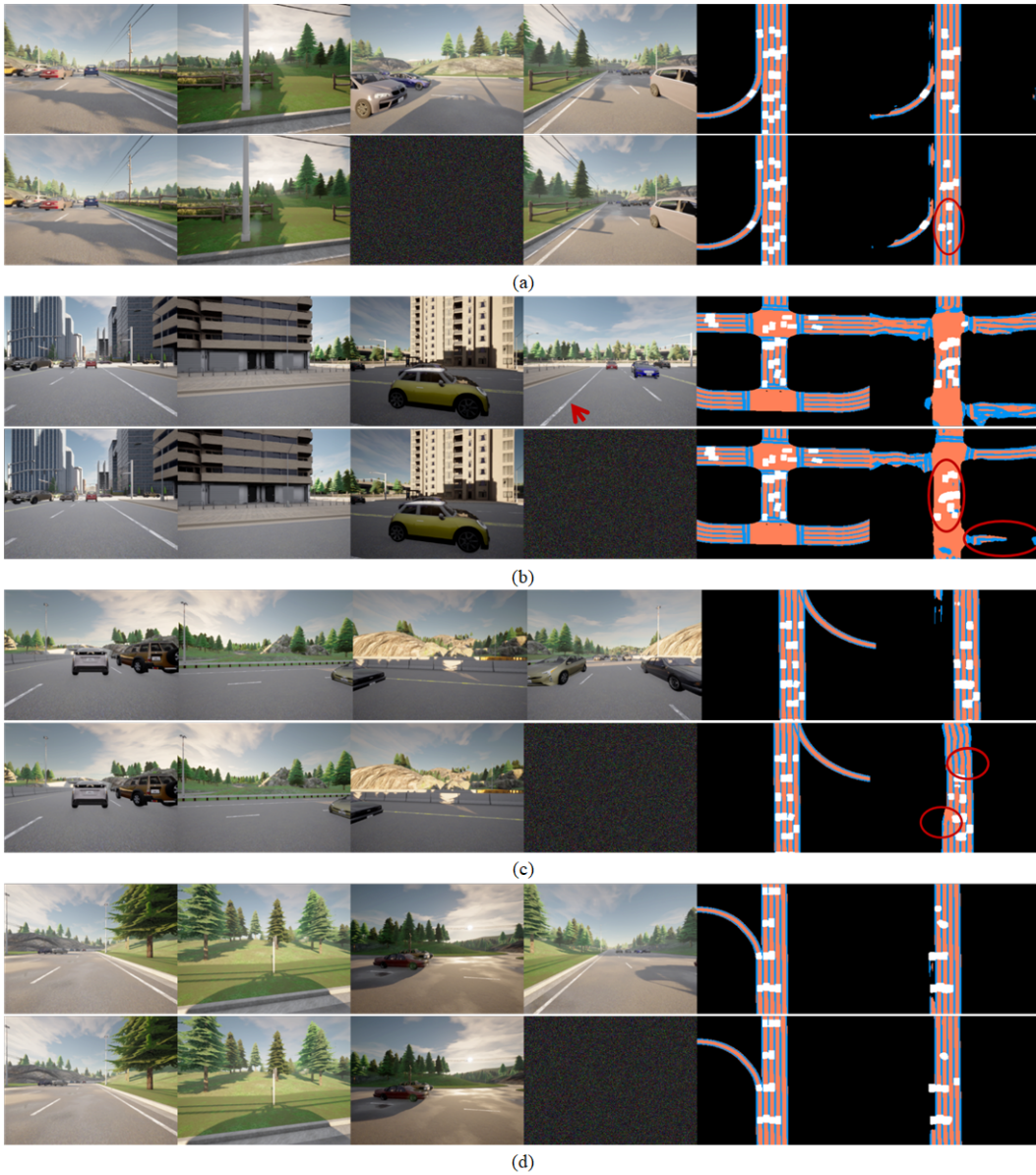


Figure 9: Visualization of different performance degradation with random noisy camera data.

Table 3: The validation experiments on whether random noise will affect collaborative perception systems. Note that we utilize the current SOTA map-segmentation method, CoBEVT.

OPV2V-N	w. random noisy	w.o. random noisy
Dr. Area	49.37	52.64
Lanes	34.80	37.96
Dynamic Veh.	39.81	47.49

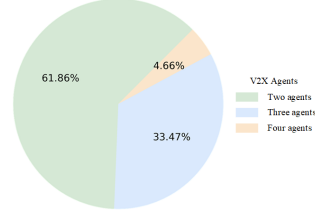


Figure 10: The distributions of V2X collaborative agents.

B Detailed Information about Experiments

B.1 Implementation Details.

For collaborative perception part, we assume all the AVs have a 70m communication range following[43], and all the vehicles out of this broadcasting radius of ego vehicle will not have any collaboration. We compare with the state-of-the-art multi-agent perception algorithms: F-Cooper, AttFuse, V2VNet, DiscoNet and CoBEVT *w.o/w.* the proposed RCDN.

Meanwhile, to make a fair comparison, we first employ CVT to extract the BEV feature from camera rigs for all methods. The transmitted BEV intermediate representation has a resolution of $32 \times 32 \times 128$; For collaborative neural fields part, we pretrain the BEV decoder with the mcp encoder for better performance, and the geometry collaborative volume feature has a resolution of $128 \times 128 \times 128$. Same as [69], we select $(t - 1, t, t + 1)$ as the mini training unit and train the whole model with the Adam[70] optimizer and cosine annealing learning rate scheduler with initial learning rate of $5e-4$ on a single RTX 3090 24G GPU with AMD Ryzen Threadripper 3960X. As for the inference time, we record the corresponding time in Table 4. Note that chunk is the smallest unit of parallel processing of the image, *e.g.*, if the image size is $(400, 400)$, the chunk size is 4096 pixels, the number of each image’s parallel chunks is about 40.

Table 4: Inference time for each chunk.

Modules	Time Cost
f_{static}	$4.47 \pm 0.11ms$
$f_{dynamic}$	$3.94 \pm 0.21ms$
f_{render}	$20.98 \pm 0.22ms$

B.2 Discussion on RCDN.

Theoretically, the RCDN reconstructs the entire collaborative scenario field, according to radial field theory[50], so whichever camera has the noise problem can actually be recovered. In this regard, we experimentally validate the RCDN using CoBEVT and V2VNet, and the corresponding results are in Table 5. We can see that i) if all the RCDN reconstructed cameras are used, the performance is much better compared to using all the noisy camera data, *e.g.* as for CoBEVT, about 62.38%/123.29%/262.70% increment for the Dr. area, lanes and dynamic vehicles, respectively. ii) compared to using all normal cameras, using all reconstructed RCDN cameras will degrade the performance, *e.g.*, as for V2VNet, about 20.94%/21.70%/35.73% decrement for the Dr. area, lanes and dynamic vehicles, respectively. To address this phenomenon, we visualize the perspective of the reconstructed camera views, shown in Figure 11, and it is not difficult to find that there is a domain gap[18, 71] between the reconstructed and the normal cameras. Meanwhile, the backbone used to extract the BEV is trained by using the normal camera, so if all reconstructed cameras are used, it does cause a certain degree of degradation. Thanks to the

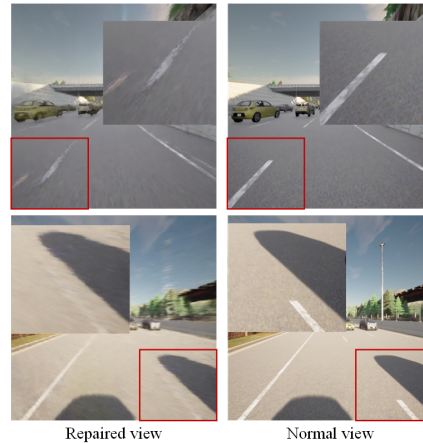


Figure 11: Visualization of domain gap between normal view and RCDN repaired view.

development of abnormal detection algorithms[72, 73], it is easy to find noisy camera data. Hence, we only replace the corresponding noisy data without replacing all data for better performance.

Table 5: Performance comparison (Dr. Area/Lanes/Dynamic Veh.)

methods/setting	all Nor. data	all RCDN data	all noisy data
CoBEVT	51.96/34.19/56.61	36.78/20.90/44.54	22.65/9.36/12.28
V2VNet	41.70/27.14/42.57	32.97/21.25/27.36	18.12/8.76/6.78

B.3 Benchmarks

We conduct extensive experiments on current collaborative perception methodologies with the proposed RCDN. Table 6 presents the segmentation performance under the expectation of random noisy camera numbers from 0 to 3 on OPV2V-N, which corresponds to the numerical results shown in Figure 3 in the main text. We see that RCDN can be portable to other baseline methods and stabilize the performance even under the extreme camera-insensitivity setting. We also visualize some training scene samples, shown in Figure 12.

Table 6: Performance of RCDN with other baseline methods. Note that – represents the failed results.

Method	Performance	Dr. Area/Lanes/Dynamic Veh.											
		w.o. RCDN						w. RCDN					
		n=0	n=1	n=2	n=3	n=0	n=1	n=2	n=3				
F-Cooper	scene1	34.03/17.55/55.56	19.37/6.67/28.96	20.41/7.77/24.39	22.68/9.27/17.56	34.03/17.55/55.56	35.46/16.82/52.69	36.85/16.23/44.45	35.31/16.88/43.49				
	scene2	48.14/24.45/55.32	44.55/16.81/20.89	35.79/17.10/24.98	35.83/16.34/22.39	48.14/24.45/55.32	48.50/24.75/52.66	47.54/22.84/52.86	46.90/19.58/54.19				
	scene3	35.00/29.86/66.79	25.43/18.01/38.00	26.11/14.99/26.28	21.94/11.56/24.74	35.00/29.86/66.79	35.93/30.10/67.70	34.40/29.51/61.14	36.77/28.86/67.09				
	scene4	65.36/63.79/77.24	30.95/17.74/31.34	27.02/18.48/16.31	-/-/7.03	65.36/63.79/77.24	64.98/62.73/77.77	65.93/62.15/67.66	-/-/70.18				
	scene5	44.67/30.20/61.74	24.03/20.50/29.32	25.57/15.51/15.49	24.03/17.55/17.32	44.67/30.20/61.74	39.56/26.73/58.00	38.20/23.83/52.49	38.51/19.31/52.02				
	Avg	45.44/33.17/63.33	28.87/15.95/29.70	26.98/14.77/21.49	26.12/13.68/17.808	45.44/33.17/63.33	44.89/32.23/61.76	44.58/30.91/55.72	39.37/21.16/57.39				
AttFuse	scene1	32.29/20.38/43.32	19.07/14.04/26.07	17.58/10.94/14.55	17.28/12.77/11.68	32.29/20.38/43.32	29.32/17.16/42.11	28.25/15.05/37.25	27.05/16.39/35.11				
	scene2	49.38/20.84/52.16	35.85/16.16/20.36	30.96/18.91/10.93	27.28/17.40/12.14	49.38/20.84/52.16	51.08/22.75/47.93	53.02/26.69/41.57	53.15/26.38/40.16				
	scene3	38.79/32.05/57.73	32.64/26.01/36.76	30.67/24.36/22.91	25.48/17.04/15.75	38.79/32.05/57.73	38.19/29.78/56.18	36.75/28.60/46.56	38.86/31.12/42.80				
	scene4	58.33/57.97/63.95	24.26/14.31/20.98	19.26/12.38/14.84	-/-/9.18	58.33/57.97/63.95	58.65/55.44/63.11	54.56/48.79/60.59	-/-/62.64				
	scene5	49.18/37.55/53.56	28.15/23.32/19.65	23.22/18.34/18.09	23.15/18.47/19.30	49.18/37.55/53.56	44.65/32.35/51.41	41.89/25.55/47.17	39.74/21.54/46.21				
	Avg	45.59/33.76/54.14	27.99/18.77/24.76	24.34/16.99/16.26	23.30/16.42/13.61	45.59/33.76/54.14	44.38/31.50/52.15	42.89/28.94/46.63	39.70/23.86/45.38				
DiscoNet	scene1	45.31/23.68/43.26	15.73/6.68/7.47	11.85/7.38/3.71	13.15/9.24/5.35	45.31/23.68/43.26	34.20/19.25/38.88	30.34/13.73/38.84	23.42/7.85/22.83				
	scene2	36.58/8.20/37.10	31.87/8.96/11.59	24.74/10.80/11.43	22.70/11.36/7.62	36.58/8.20/37.10	33.60/8.37/34.90	35.72/11.28/32.53	30.72/11.83/29.87				
	scene3	28.61/17.05/35.23	19.51/10.48/25.00	14.87/25.98/3.56	14.42/8.73/-	28.61/17.05/35.23	28.89/18.44/28.63	25.98/16.46/22.40	27.33/18.86/21.04				
	scene4	50.28/37.95/62.15	32.42/20.69/11.13	24.30/12.44/7.84	-/-/3.46	50.28/37.95/62.15	49.50/38.23/59.25	51.25/40.25/55.49	-/-/54.21				
	scene5	50.74/34.33/55.07	22.03/14.64/13.54	22.59/13.58/16.91	27.55/14.70/14.06	50.74/34.33/55.07	46.50/30.58/53.51	41.86/28.56/48.83	44.22/25.07/48.82				
	Avg	42.30/24.24/46.56	24.31/12.29/9.25	19.67/14.04/8.69	21.25/12.32/6.10	42.30/24.24/46.56	38.54/22.97/43.03	37.03/22.06/39.62	37.33/23.10/35.35				
V2VNet	scene1	39.83/19.49/28.06	20.52/7.15/8.21	11.41/7.68/5.68	9.54/7.33/3.94	39.83/19.49/28.06	39.28/19.95/28.72	36.13/15.55/28.25	30.56/15.21/19.67				
	scene2	40.21/14.45/39.60	37.38/7.19/14.73	29.05/6.84/6.77	19.64/6.66/8.58	40.21/14.45/39.60	38.45/14.96/39.45	34.61/8.07/39.17	33.40/12.29/33.17				
	scene3	33.24/26.83/31.89	20.11/6.11/2.93	12.39/7.28/8.37	9.48/7.01/1.49	33.24/26.83/31.89	29.53/20.95/35.15	24.75/16.82/26.92	27.94/16.59/20.52				
	scene4	49.76/36.24/57.83	28.50/17.23/11.52	26.74/18.85/9.37	14.54/12.00/8.00	49.76/36.24/57.83	48.34/36.74/58.46	47.00/36.37/57.31	53.40/40.01/56.45				
	scene5	45.47/38.71/55.45	33.46/14.91/18.99	29.66/17.04/16.38	24.23/14.99/14.10	45.47/38.71/55.45	42.98/33.59/52.06	39.04/28.94/52.93	39.21/28.99/47.79				
	Avg	41.70/27.14/42.57	27.99/10.52/11.28	21.85/11.54/9.31	15.49/9.60/7.22	41.70/27.14/42.57	39.72/25.24/42.77	36.31/21.15/40.92	36.90/22.62/35.52				
CoBEVT	scene1	30.59/12.43/47.62	24.55/10.07/30.67	23.23/8.19/18.83	22.99/11.63/14.59	30.59/12.43/47.62	27.37/10.63/46.65	27.22/11.31/41.38	26.96/10.59/36.99				
	scene2	39.28/10.72/54.25	37.47/14.26/28.43	32.32/12.94/16.27	23.43/8.41/11.93	39.28/10.72/54.25	37.47/9.64/50.48	44.97/15.85/49.88	39.51/9.77/46.46				
	scene3	47.80/37.85/60.40	24.91/11.90/33.73	18.34/11.15/18.29	15.78/11.56/63.49	47.80/37.85/60.40	49.45/37.51/60.02	50.96/40.09/57.53	49.85/37.13/63.49				
	scene4	73.62/61.44/61.70	46.69/20.88/38.91	34.26/12.43/12.10	-/-/8.67	73.62/61.44/61.70	70.27/59.07/62.01	68.48/56.13/53.58	-/-/56.71				
	scene5	68.50/48.53/59.06	26.80/15.13/30.32	28.38/8.42/14.19	23.51/11.26/10.67	68.50/48.53/59.06	51.39/30.88/56.35	52.02/30.53/51.86	46.52/25.31/53.37				
	Avg	51.96/34.19/56.61	32.08/14.45/32.41	27.31/10.63/15.99	22.05/10.53/11.52	51.96/34.19/56.61	47.19/29.55/55.10	48.73/30.78/50.85	46.10/27.78/51.40				

B.4 PSNR Results

We also record the corresponding PSNR results of different baseline methods *w.* RCDN’s reconstruction’s image view, as shown in Table 7. Note that the term peak signal-to-noise ratio (PSNR) is an expression for the ratio between the maximum possible value (power) of a signal and the power of distorting noise that affects the quality of its representation. Hence, the higher PSNR, the better image quality.

B.5 Geometry BEV Volume Feature

We utilize the geometry BEV volume feature to speed up the training process and improve the generality of the collaborative neural fields. We observe that with f_{geo_bev} the RCDN can obtain higher PSNR initial values and a shorter training process, as shown in Figure 13.

Table 7: The PSNR results.

	PSNR
F-Cooper	26.11
AttFuse	25.79
DiscoNet	25.86
V2VNet	26.14
CoBEVT	25.89



Figure 12: Visualization of some training scenes samples. Note that we cover the classical scenes, including the four-way Intersection, T Intersection, Midblock, Entrance Ramp and Curvy Segment.

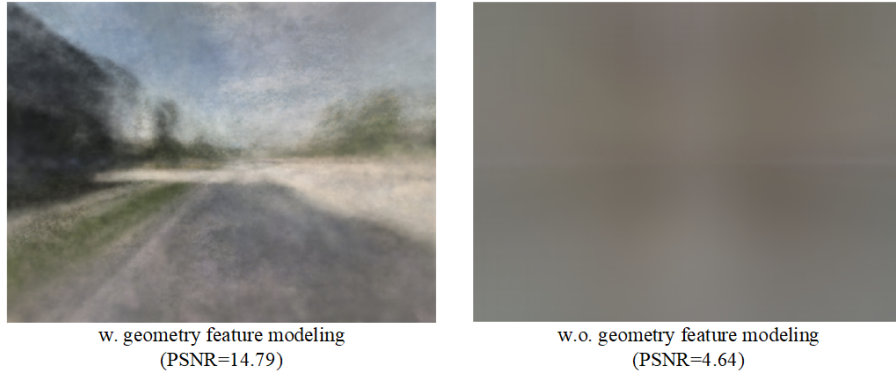


Figure 13: Visualization of *w.o/w.* geometry BEV volume feature modeling.

B.6 Loss Functions

Similar to [68], we regularize the collaborative scene flow to be spatially smooth by minimizing the difference between neighboring 3D points' scene flow. To regularize the consistency of the collaborative scene flow, we have the scene flow cycle consistency regularization as follows:

$$\mathcal{L}_{cyc} = \sum \|\mathbf{s}_{fw}(\mathbf{r}, t) + \mathbf{s}_{bw}(\mathbf{r} + \mathbf{s}_{fw}(\mathbf{r}, t), t + 1)\|_2^2 \quad (13a)$$

$$+ \sum \|\mathbf{s}_{bw}(\mathbf{r}, t) + \mathbf{s}_{fw}(\mathbf{r} + \mathbf{s}_{bw}(\mathbf{r}, t), t + 1)\|_2^2 \quad (13b)$$

As for the weights of different losses in Eq 12, we set $\lambda_1, \lambda_2, \lambda_4 = 1.0$ and $\lambda_3 = 0.1$ for training. Meanwhile, we train the whole network for about 1000 epochs, which takes about 20 to 30 minutes.

C Visualization

We visualize some segmentation results of different baseline methods *w.o/w* RCND under the different scenes, shown in Figure 14-18.

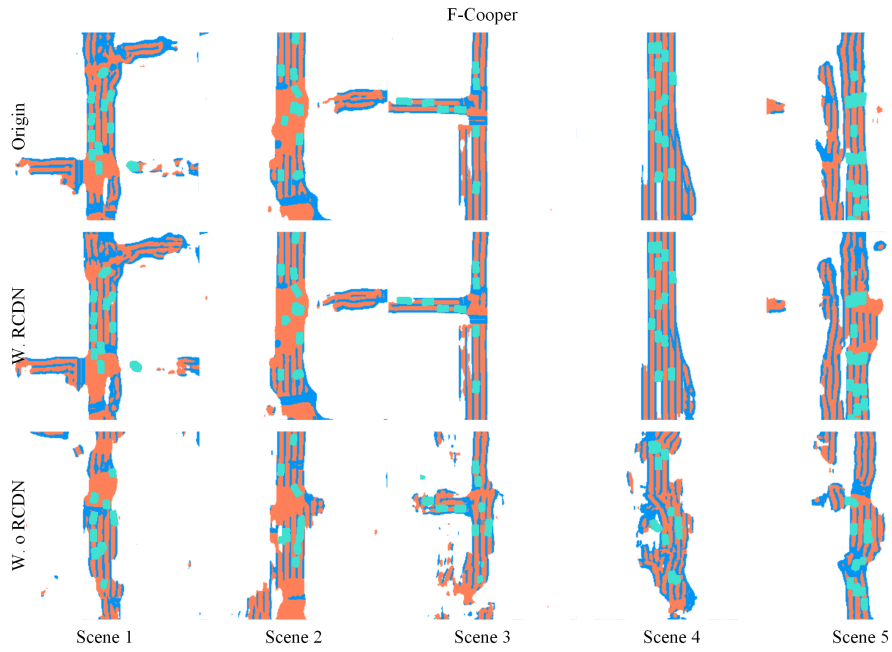


Figure 14: Visualization of baseline method of F-Cooper *w.o/w*. RCDN with one random camera failure.

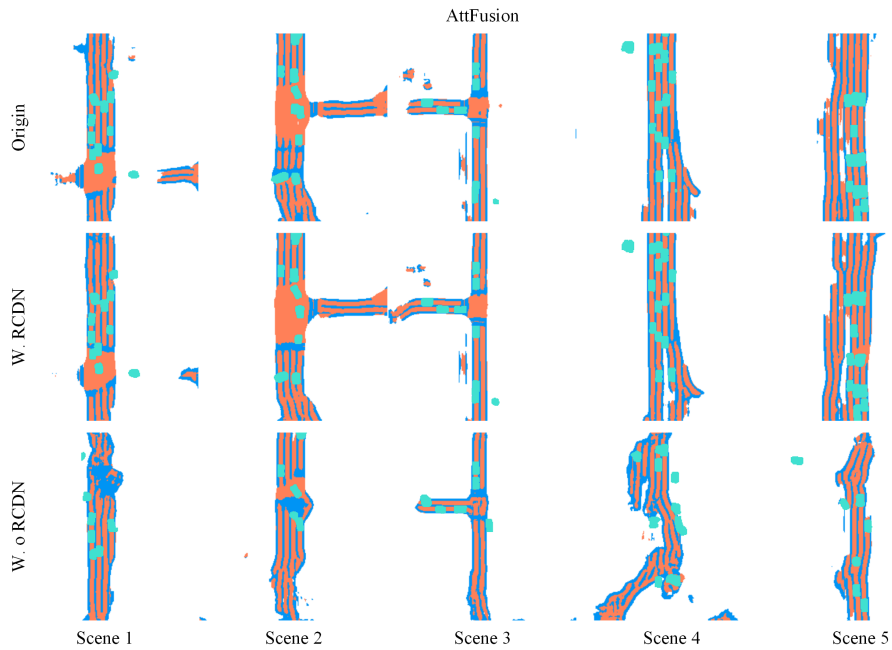


Figure 15: Visualization of baseline method of AttFuse *w.o/w*. RCDN with one random camera failure.

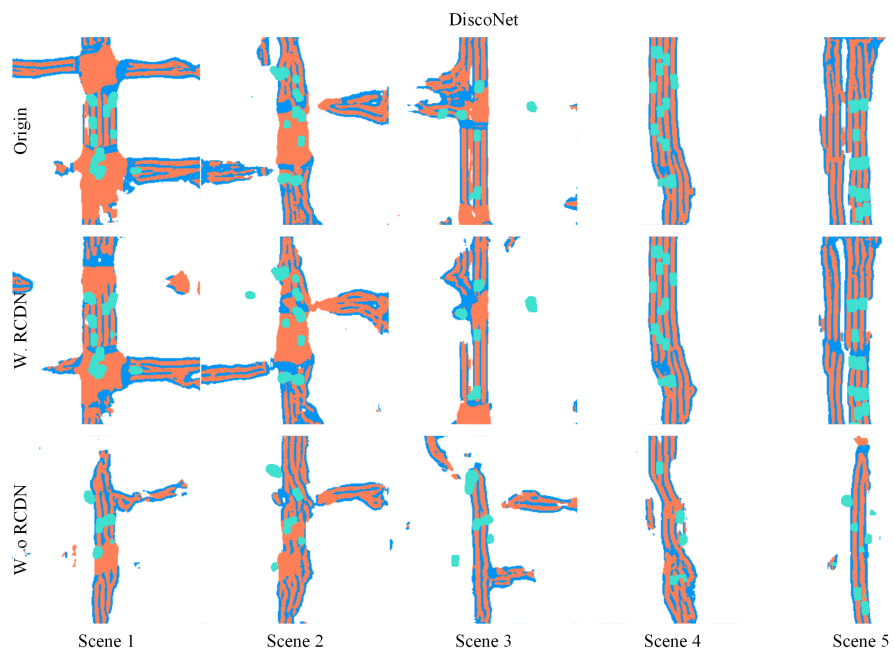


Figure 16: Visualization of baseline method of DiscoNet *w.o/w.* RCDN with one random camera failure.

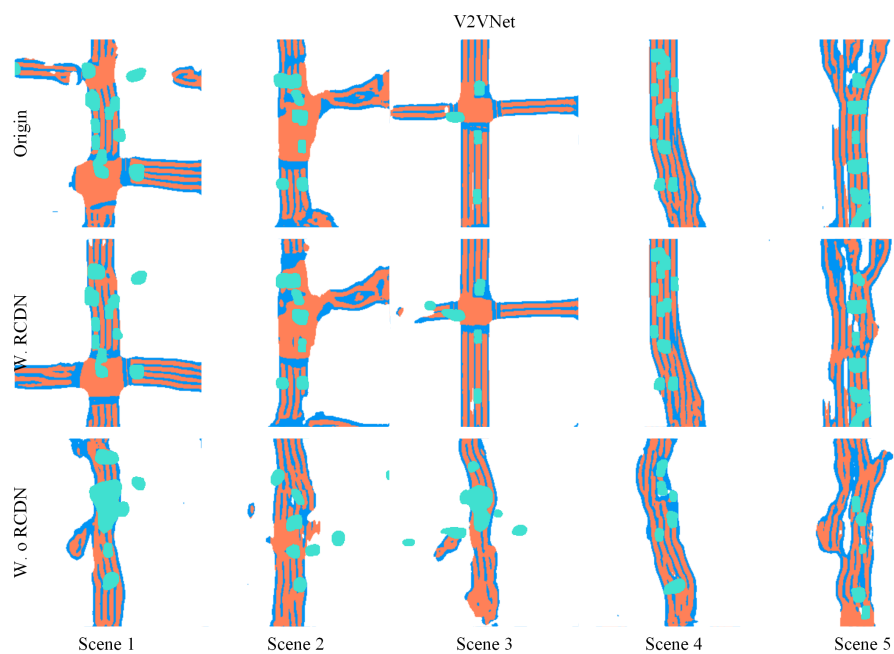


Figure 17: Visualization of baseline method of V2VNet *w.o/w.* RCDN with one random camera failure.

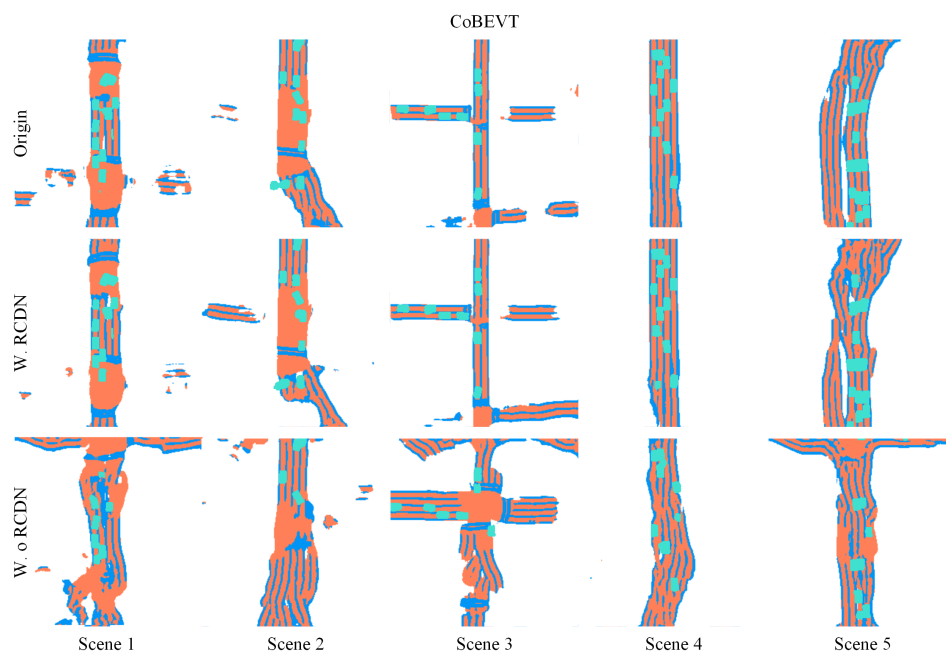


Figure 18: Visualization of baseline method of CoBEVT *w.o/w.* RCDN with one random camera failure.